RSC Advances

ROYAL SOCIETY OF CHEMISTRY

www.rsc.org/advances

Physicochemical studies toward the removal of Zn(II) and Pb(II) ions through adsorption on montmorillonite-supported zero-valent iron nanoparticles

Jiao Wang [a,b], Guijian Liu [a,b *], Tanfu Li [a], Chuncai Zhou [a]

[a] *CAS Key Laboratory of Crust-Mantle Materials and the Environments, School of Earth and Space Sciences, University of Science and Technology of China, Hefei 230026, China*

[b] *State Key Laboratory of Loess and Quaternary Geology, Institute of Earth Environment, The Chinese Academy of Sciences, Xi'an, Shaanxi 710075, China*

* Corresponding author. Tel: +86-551-63603714; fax: +86-551-63621485.

E-mail address: lgj@ustc.edu.cn (G.J. Liu)

Abstract: This study reports the adsorption of Zn(II) and Pb(II) on montmorillonite-supported zero-valent iron nanoparticles (nZVI-Mont). The kinetics of Zn(II) and Pb(II) adsorption were evaluated for various contact times. The adsorption of Zn(II) and Pb(II) at different initial concentrations was examined by injecting 0.5 g of adsorbents to achieve equilibrium. The adsorption of Zn(II) and Pb(II) was an exothermic process. The pseudo-second-order kinetic model fits well with the adsorption of Zn (II) and Pb (II) (r^2> 0.99 at all temperatures tested). The Zn(II) adsorption process was a simultaneously physical and chemical process, fitting the Freundlich (r^2=0.981), Temkin (r^2=0.983) and the D–R isotherm models (r^2=0.988) well. However, the Pb(II) adsorption only fit the Freundlich isotherm model. The activation energies of the Zn(II) adsorption onto nZVI-Mont was range from 11.71 kJ mol^{-1} to 46.37 kJ mol^{-1} and the activation energies of the Pb(II) adsorption onto nZVI-Mont was range from 0.26 kJ mol^{-1} to 17.67 kJ mol^{-1}. The negative values for the Gibbs free energy (ΔG^o) and enthalpy of adsorption (ΔH^o) revealed that the adsorption process was spontaneous and exothermic, respectively. In addition, the adsorption mechanisms for Zn(II) and Pb(II) are significantly different.

Keywords: nZVI-Montmorillonite; Zinc and lead; Adsorption; Activation energy; Thermodynamics

1. Introduction

Metal ions are discharged extensively from various modern industries, such as the steel, metallurgy, machine, electrical, chemical, light, military and medical industries [1-4]. These Metal ions can accumulate in the environment, damage the environmental balance and potentially threaten human health [5]. Zinc and lead are examples of such metal ions. Zinc is an essential nutrient for plant and animal metabolism that regulates many biochemical processes in the human body [6], but excessive amounts of zinc also cause serious health problems, negative effects on human health (stimulating the gastrointestinal tract and skin) [7-8]. Zinc enters the environment through the combustion of fossil fuels, metal production, electroplating, and the manufacture of batteries, pigments, and screens [9]. Lead is extremely toxic and can damage the nervous system, kidneys and reproductive system, particularly in children [10]. This metal is widely applied in the sulfuric acid industry, as well as in batteries, cable sheathing, gasoline antiknock additives, pigments and anti-corrosion linings for industrial metallurgy equipment [11]. Therefore, zinc and lead are priority pollutants according to the US Environmental Protection Agency [12]. Large amounts of wastewater containing high concentrations of zinc and lead have been produced every day, possibly polluting the surface and groundwater directly or indirectly [13]. Toxic elements are absorbed by organisms and are later accumulated and biomagnified in biotic communities.

The chemical treatments for removing heavy metals include several methods, such as precipitation, solvent extraction, ion-exchange [14] and adsorption [15]. Adsorption is an inexpensive process that has become an efficient method for removing heavy metals. Various adsorbents, including clays, zeolites, biomass, microorganism, metal oxides, lime and calcium carbonate, fly ash, activated carbon and nanoscale zero-valent iron (nZVI) have been tested for Zn(II) and Pb(II) removal [6,16-23]. Recently, a new composite material called montmorillonite-supported zero-valent iron nanoparticles (nZVI-Mont) has become highly promising due to its nanoparticle size, large surface area and high density of reactive sites [24-26], leading to a high removal efficiency. In addition, the nZVI-Mont could be separated easily from water and adsorbate when exposed to a proper magnetic field. The adsorption mechanism is related to the standard redox potential of the contaminant. The standard redox potentials of Zn(II) (-0.76 V, 298.15 K) and Pb(II) (-0.13 V, 298.15 K) are negative or slightly more positive, respectively than zero-valent iron (-0.41 V, 298.15 K); therefore, the conceptual model for Zn(II) removal using nZVI will only involve

adsorption, but Pb(II) removal involves both adsorption and reduction [27]. Boparai et al. [28] indicated that the adsorption of Cd(II) on nZVI particles follows pseudo-second-order kinetics, and the adsorption isotherm data could be described by the Langmuir and Temkin equations. The Freundlich equation was used to model Pb(II) adsorption on amino-functionalized nZVI particles [29]. To date, Zn(II) adsorption onto nZVI-Mont has not been studied in detail.

Therefore, a detailed study was conducted to explore the adsorption characteristics of aqueous Zn(II) by nZVI-Mont. Before designing the adsorption scheme, the adsorption mechanism and kinetics were investigated. The adsorption isotherms or adsorption capacity at equilibrium can be used to predict the optimal conditions for maximum removal by nZVI-Mont. Pb(II) was adopted for comparison when nZVI-Mont became a useful adsorbent for capturing the Zn(II) and Pb(II) in contaminated water. The aims of the present study were as follows: (i) synthesize and characterize nZVI-Mont, (ii) examine different mathematical models of Zn(II) and Pb(II) adsorption and the changes in the thermodynamics of the adsorption process, (iii) to evaluate the nature of the absorption of Zn(II) and Pb(II) on nZVI-Mont particles at equilibrium, and (iv) explore the potential synergic effects of nZVI and montmorillonite. A critical interpretation of the adsorption kinetics, mechanism and thermodynamics changes will provide beneficial information for finding applications of nZVI-Mont.

2. Materials and methods

2.1 Materials

2.1.1 Preparation and characterization of adsorbent

nZVI-Mont was prepared by performing a liquid-phase reduction under ambient atmosphere using sodium borohydride, according to the previously published method [30] with some modifications. First, 19.36 g of $FeCl_3 \cdot 6H_2O$ were added to a mixture containing 2.0 g of montmorillonite which was full exchanged by Na^+ and uniformly dispersed in 100 ml of deionized water. To generate a good dispersion and ensure the replacing of Na^+ by Fe(III), the mixture was magnetically stirred for approximately 12 h. Simultaneously, 10.84 g of solid $NaBH_4$ were dissolved in 100 ml of deionized water, maintaining a specific B/Fe ratio of 4:1. When a drop of the fresh $NaBH_4$ solution was introduced, black nZVI particles immediately appeared, indicating the restoration of Fe(III) (on montmorillonite / in solution). Consistent stirring was required to disperse the reaction mixture

evenly. The synthesized material was separated through centrifugation at 3000 rpm for 40 minutes. The products were thoroughly rinsed via centrifugation, dispersed in 50 vol% ethanol solution and rinsed twice washed in acetone. Finally, the prepared material was dried overnight under vacuum at 60 ℃. Theoretically, the main reaction in the process is the following [31]:

$$4Fe^{3+} + 3BH^{-}_{4} + 9H_2O \rightarrow 4Fe^{0}(s) \downarrow + 3B(OH)_3 + 9H^{+} + 6H_2(g) \uparrow$$

The materials were characterized using X-ray diffraction (XRD) (Rigaku Dmax 12KW diffraction machine, Japan), transmission electron microscopy (TEM) (H-8100, Japan's Hitachi LTD, Japan).

2.1.2 Adsorbate (Zn(II) and Pb(II)) and other chemicals

All of the reagents used in this study were analytical grade. Iron (III) chloride hexahydrate ($FeCl_3$•$6H_2O$, Shangha–China) and sodium borohydride ($NaBH_4$) were the primary reagents used. The standard solutions of Zn(II) and Pb(II) (Shangha–China) were diluted to 1000 mg/L with deionized water that was acidified with small amount of nitric acid. The concentrations of the Zn(II) and Pb(II) were determined using Inductively Coupled Plasma Optical Emission Spectroscopy (ICP-OES). The pH was adjusted by adding a known amount of NaOH and HNO_3 solutions and was estimated using pH test strips.

2.2 Adsorption experiments

Zn(II) or Pb(II) solutions with concentrations of 25, 50, 75, 100 and 125 mg/L were generated from the stock solution through dilution. Subsequently, 0.5 g of the adsorbent was added to 100 ml of a 50 mg/L solution of Pb(II) or Zn(II). A 125 ml high-density poly (ethylene) (HDPE) bottle was used during the experiment. All of the bottles were placed in a homothermal shaking water bath. The adsorption kinetics was determined using a batch procedure from 288 K to 313 K at pH 5.0. Samples were collected at 0-120 minutes or 0-400 minutes for Zn(II) and Pb(II) analysis. Blank experiments were performed concurrently.

The adsorption isotherm was obtained by placing 100 ml of solution into a HDPE bottle containing 0.5 g nZVI-Mont at 298K. The initial concentration was set as 25, 50, 75, 100 or 125 mg/L. Samples were collected at 120 min or 400 min to measure the final concentration of Zn(II) and Pb(II). Batch experiments were performed in duplicates, and the data used to match the curves were the average values.

Samples from the mixture, which was strongly shaken, were taken using a 3 ml HDPE syringe and filtered through 0.2 μm cellulose acetate syringe filters at the end of the contact process. The

supernatant was collected, acidified and analyzed by ICP-OES. The following formulas were used for the corresponding calculations:

$$q = (C_0 - C_t) / m, \quad (1)$$

$$E = ((C_0 - C_t) / C_0) \times 100. \quad (2)$$

where C_0 and C_t (mg/L) are the initial and final concentration of Zn(II) and Pb(II), respectively, and m (g) is the amount of adsorbent in 1 L of solution. E (%), is the removal efficiency of Zn(II) and Pb(II).

2.3 Adsorption kinetics theory

As the most popular kinetics equation [32], the pseudo-first-order kinetics equation describes the adsorption in solid–liquid systems based on the sorption capacity of solids [33]. The pseudo-first-order kinetics model assumes that one ion is adsorbed onto one unoccupied adsorption site on the nZVI-Mont surface [28]. The pseudo-second-order kinetics equation represents a chemisorption process from liquid solutions [34]. The related equations and parameters are expressed as follows.

2.3.1 Pseudo-first-order kinetics

The general formula is as follows:

$$\frac{dq_t}{dt} = k_1 (q_e - q_t), \quad (3)$$

where q_e and q_t (mg g^{-1}) are the adsorption capacities at equilibrium and t respectively, and k_1 is the pseudo-first-order rate constant (min).

The linear form of the pseudo-first-order model can be expressed as follows [35]:

$$\log(q_e - q_t) = \log q_e - \frac{k_1}{2.303} t \quad (4)$$

2.3.2 Pseudo-second-order kinetics

The general formula is expressed as follows [35]:

$$\frac{dq_t}{dt} = k_2 (q_e - q_t)^2, \quad (5)$$

where q_e and q_t (mg g^{-1}) are the adsorption capacities at equilibrium and t, respectively, k_2 (g mg^{-1} min^{-1}) is the rate constant for pseudo-second-order adsorption, and $k_2 q_e^2$ (mg g^{-1} min^{-1}) is the initial adsorption rate.

The linear form of pseudo-second-order model can be expressed as follows [36]:

$$\frac{t}{q_t} = \frac{1}{k_2 q_e^2} + \frac{1}{q_e} t \quad (6)$$

2.3.3 The assessment of adsorption dynamics model fitting

The linear correlation (r^2) and non-linear Chi-square (χ^2) coefficients were used to assess the fits. The correlation coefficient is used to reflect the correlation and closeness of the variables. This value is a statistical indicator that is calculated through a covariance method based on the deviation between two variables and their average; therefore, this value reflects the degree of correlation between the two variables. The other method is chi-squared test, which measures the difference between the experimental and modelled data.

The mathematical form of the Chi-squared test can be expressed as follows [37]:

$$\chi^2 = \sum \frac{(q_{e,exp} - q_{e,cal})^2}{q_{e,cal}} \quad (7)$$

where $q_{e,exp}$ is the experimentally determined equilibrium capacity and $q_{e,cal}$ is the simulated equilibrium capacity. If the simulated data are similar to the experimental data, χ^2 will be small, while if they differ, χ^2 will be large.

2.4 Adsorption isotherm models

2.4.1 Langmuir isotherm

The Langmuir isotherm assumes that the surface is uniform. The number of adsorption sites is finite, and a site cannot be occupied by a new molecule unless the adsorbed molecule leaves. This model describes a monolayer adsorption process equilibrium when the maximum adsorption rate equals the maximum sorption rate. No forces exist between adsorbed molecules on the surface of solid. The linear form of the Langmuir isotherm model is expressed as follows [38]:

$$\frac{C_e}{q_e} = \frac{1}{K_L q_m} + \frac{C_e}{q_m} \quad (8)$$

where K_L is the Langmuir constant related to the energy of adsorption, and q_m is the maximum adsorption capacity (mg g^{-1}).

2.4.2 Freundlich isotherm

Both chemisorption (monolayer) and physisorption (multilayer) can be described using the Freundlich isotherm. This model is based on the heterogeneous adsorption equilibrium on the surface of an adsorbent [39]. The linear form of the Freundlich equation is as follows [40]:

$$\log q_e = \log K_F + \frac{1}{n} \log C_e \quad (9)$$

where K_F and n are the Freundlich isotherm constants related to adsorption capacity and adsorption intensity, respectively, and C_e is the equilibrium concentration (mg L^{-1}).

2.4.3 Temkin isotherm

The Temkin isotherm model assumes that the adsorption energy decreases linearly with the surface coverage due to the adsorbent–adsorbate interactions. The linear form of the Temkin isotherm model is written as follows [41]:

$$q_e = \frac{Rt}{b} \ln K_T + \frac{RT}{b} \ln C_e \quad (10)$$

where b is the Temkin constant related to the heat of adsorption (J mol^{-1}), and K_T is the Temkin isotherm constant (L g^{-1}).

2.4.4 Dubinin–Radushkevich (D–R) isotherm

The D-R isotherm model assumes that the adsorption is multilayered, involves van der Waals forces and is applicable for physical adsorption processes [42]. The equation is as follows [43]:

$$\ln q_e = \ln q_d - \beta\varepsilon^2 \quad (11)$$

Where q_d is the D–R constant (mg g^{-1}), and β is a constant related to free energy. ε is the Polanyi potential, which is defined as:

$$\varepsilon = RT \ln \left[1 + \frac{1}{C_e}\right] \quad (12)$$

2.5The Arrhenius equation

The Arrhenius equation for calculating adsorption activation energy is expressed as [44]:

$$k_2 = k \exp\left(-\frac{E_a}{RT}\right) \quad (13)$$

Where k is the temperature-independent factor (g $mg^{-1}h^{-1}$), E_a the activation energy of sorption (kJ mol^{-1}), R the universal gas constant (8.314 J $mol^{-1}K$) and T the solution temperature (K).

2.6 Adsorption mechanism and intraparticle diffusion

The adsorption mechanism of Zn(II) and Pb(II) was followed the steps below [45, 46]:

(i) the migration of the metal ions from the solution to the surface of the adsorbent;

(ii) the diffusion of metal ions through the boundary layer to the surface of adsorbent;

(iii) intraparticle or pore diffusion, where the adsorbate molecules move inside of the adsorbent particles;

(iv) the adsorption of metal ions at an active site on the interior of adsorbent.

During solid/liquid sorption processes, the solute transfer is usually characterized by the external

mass transfer (boundary layer diffusion), intraparticle diffusion or both [16]. We can fit an intraparticle diffusion plot to identify the adsorption mechanism. The intraparticle diffusion model is based on the Weber–Morris intraparticle diffusion equation [47]:

$$q_t = k_i t^{0.5} + C \quad (14)$$

where k_i is the intraparticle diffusion rate constant (mg $g^{-1}min^{0.5}$), and C is the intercept.

2.7 Thermodynamic study

Thermodynamic parameters including the standard Gibbs free energy ΔG^o (kJ mol^{-1}), standard enthalpy change (ΔH^o) and standard change in entropy (ΔS^o) for the adsorption of Zn(II) and Pb(II) on nZVI-Mont have been determined using the following equations [48, 49]:

$$\Delta G^o = -RTlnK_o \quad (15)$$

$$\ln K_o = \frac{\Delta S^o}{R} - \frac{\Delta H^o}{RT} \quad (16)$$

K_o can be simplified when the activity coefficients approach unity at very low concentrations [36, 50]:

$$\lim_{c_{s\to 0}} K_0 \approx \frac{a_s}{a_e} = \frac{C_s}{C_e} \quad (17)$$

where a_s is the Zn(II) and Pb(II) activity of adsorption on nZVI-Mont, a_e is the Zn(II) and Pb(II) activity in solution at equilibrium, C_s is the amount of Zn(II) and Pb(II) adsorbed on the nZVI-Mont (mmol g^{-1}), and C_e is the concentration of Zn(II) and Pb(II) at equilibrium (mmol mL^{-1}).

3. Results and discussion

3.1. Characterization of nZVI synthesized on montmorillonite

The morphology of the montmorillonite and nZVI synthesized on the montmorillonite were analyzed using TEM (Fig. 1). The montmorillonite (Fig. 1a) had a smooth, fluctuant and layered surface. The individual particles were spherical (Fig. 1b). The synthesized nZVI exhibited a typical core-shell structure (Fig. 1c), agreeing with previous reporter [51-53]. The TEM image (Fig. 1d) revealed that most of synthesized nZVI formed spherical particles [54], and a portion of the nZVI aggregated to form chains due to the magnetic interactions between the nanoparticles [55]. The XRD patterns of freshly synthesized nZVI were shown in Fig. 2, revealing that Fe^0 at a 2-theta value of 44.9° was the major state of iron. The nZVI showed very weak oxide signals (hematite at 22.5° 2-theta, hematite/magnetite at 36° 2-theta, lepidocrocite at 47° 2-theta) in the

XRD pattern, indicating that the material was mildly oxidized during preparation. The magnetite and maghemite in the samples cannot be clearly distinguished using the XRD patterns, similar to previous reports [56, 57]. The inset shows that the supporting material contains primarily quartz (reflection at a 2θ value of 26.74°) and montmorillonite (reflection at 2θ of 12.5° and 20.9°). The specific BET surface area of the adsorbent was 40.1 m^2 g^{-1} versus 58.4 m^2 g^{-1} for montmorillonite, and the adsorption average pore width was 11.1 nm versus 7.1 nm for montmorillonite.

3.2 Adsorption Kinetics of Zn(II) and Pb(II)

Temperature strongly affected the adsorption capacity and the time needed to reach equilibrium. The effect of the temperature on the adsorption of Zn(II) and Pb(II) by nZVI-Mont was studied from 288 to 313 K at C_0= 50 mg L^{-1} with 5 g L^{-1} of nZVI-Mont. Fig. 3a and b show the adsorption curves for Zn (II) and Pb(II) at different times and temperatures, respectively. The equilibrium times for the Zn(II) adsorption were approximately 39.7 min, 41.6 min, 42.1 min, 42.9 min and 43.7 min at temperatures between 288 K and 313 K. In addition, the equilibrium time for the adsorption of Pb(II) was approximately 302 min at 288 K, 318 min at 293 K, 324 min at 298 K, and 335 min from 303 K to 313 K. In addition, the adsorption capacity is greater for lower temperatures for both ions, indicating that the adsorption was exothermic and remaining consistent with the previous research [19]. The relative thermodynamic parameters were discussed further, as described below. The data have been analyzed based on the pseudo-first-order and pseudo-second-order kinetic models.

3.2.1 Pseudo first-order kinetics

k_1 and q_e were evaluated using the slopes and intercepts of the linear plots of $\log(q_e - q_t)$ versus t (Fig. 4, Table 1). The linear regression coefficients (r_1^2 or r_2^2, ranging from 0.77 to 0.88) for Zn (II) seemed adequate, while those (ranging from 0.89 to 0.96) for Pb(II) were relatively high. The calculated adsorption capacity data (Table 1) for Zn (II) revealed a much lower equilibrium value for the pseudo-first-order model. However, the data calculated for Pb (II) generated a much higher equilibrium value than the experimental results. Moreover, the experimental observations are nonlinear upon close inspection, as shown in Fig. 4. This model cannot describe the adsorption of Zn (II) and Pb (II) on nZVI-Mont; therefore, this process did not follow a pseudo-first-order kinetics model.

3.2.2 Pseudo second-order kinetics

Fig. 5 shows the pseudo-second-order kinetic plots of t/q_t versus time (t) for Zn(II) and Pb(II) adsorption at different temperatures, respectively. The relative parameters $q_{e,cal}$ and k_2 (Tab. 1) can be determined from the slope and intercept of plots. These results are similar to the experimental results at each temperature; the correlation coefficients (r_2^2) are high, reaching almost 1.00). A smaller difference was observed between the fitted equilibrium adsorption capacity and the experimental value. Therefore, the adsorption of Zn(II) and Pb(II) on nZVI-Mont followed a pseudo-second-order kinetics model, and these species were adsorbed onto the surface through a chemical interaction. Similar discoveries have been reported for natural bentonite [16] and magnetite nanoparticles [19].

The χ^2 values from the pseudo-second-order model were 0.09 and 0.24 and were much lower than those of the pseudo-first-order model (10.52 and 11.51). Therefore, the adsorption of Zn(II) and Pb(II) followed a pseudo-second-order kinetics model.

3.3 Adsorption isotherms

Figures 6-7 display the adsorption equilibrium isotherms of Zn(II) and Pb(II) on nZVI-Mont, obtained at 298K and pH 5.0. Analysis of the data from different isotherm models is an important step to determine a suitable model [58]. The data have been analyzed using the Freundlich, Langmuir, Temkin, and Dubinin–Radushkevich (D–R) isotherm models.

Fig. 6a shows a plot of $\log q_e$ versus $\log C_e$ (Tab.2). K_F and n, which are the Freundlich isotherm constants; these constants are calculated from the intercept and slope separately. Some researchers believe that n indicates a high affinity between the adsorbate [59] and adsorbent in addition to the occurrence of chemisorption when greater than unity [60]. K_F is the other constant and is related to the adsorption capacity. The results revealed that Pb(II) is chemisorbed because the value of n (2.47) is greater than one. The adsorption capacity for Zn(II) is larger than that of Pb(II), as indicated by the larger K_F value (17.25>12.35).

Fig. 6b shows a plot of C_e/q_e versus C_e at 298K. K_L and q_m, are the Langmuir isotherm constants, which were calculated from the intercept and slope separately. The data are not consistent with the values determined previously using the Freundlich isotherm model. The Langmuir isotherm correlation coefficient for Zn(II) is the lowest and is not very high for Pb(II) when compared to the other three models. The Zn(II) adsorption capacity on nZVI-Mont at 298 K

was a negative value, suggesting that the Langmuir isotherm model could not be used to fit the Zn(II) adsorption on nZVI-Mont.

The Temkin isotherm model describes a chemisorption process for an adsorbate onto the adsorbent [61]. Fig. 6c and 7c show a linear plot for q_e versus $\log C_e$ at 298K. The correlation coefficients were 0.983 and 0.732 (Tab. 2). The Zn(II) adsorption on nZVI-Mont fits the Temkin isotherm model well, while the Pb(II) adsorption on nZVI-Mont does not. It indicates that the adsorption of Zn(II) onto nZVI-Mont may be a chemisorption process.

The D–R isotherm model describes a physical adsorption process. Fig. 6d and 7d displayed a linear plot for $\log q_e$ versus ε^2 at 298K. q_d and β, as main D–R isotherm parameters, were calculated separately using the intercept and slope. The correlation coefficient for Pb(II) is the lowest among the four isotherm models (Tab. 2), suggesting that the adsorption of Pb(II) onto nZVI is not a physical process [28].

Based on the analysis above, the Zn(II) adsorption on nZVI-Mont was both physical and chemical, fitting Freundlich and the D–R isotherm models well. Moreover, the Temkin isotherm model can provide a better description. Previous researchers [16, 62] have reported that Langmuir isotherms usually fit the experimental data for bentonite or magnetite better than Freundlich isotherms, which opposes the results of this study. However, the Pb(II) adsorption on nZVI-Mont involves chemisorption primarily, fitting the Freundlich isotherm model well. The other three isotherm models cannot depict this adsorption appropriately.

3.4 Adsorption activation energy

The activation energy is an important parameter used to determine the type of adsorption [63, 64]. Generally, the physical adsorption reaction was a multilayered, quick and reversible process controlled by the van der Waals force; therefore, little energy was required. The chemical adsorption reaction was monolayered, slow and process controlled by chemical bonds; therefore, larger activation energies are required. In addition, both processes may exist together.

The adsorption activation energy can be derived as a temperature-independent rate parameter using the Arrhenius equation [44]. The fits for the pseudo-second-order kinetics model provide adsorption rate constants to match Arrhenius equation. Plotting $-\ln k_2$ versus $1/\mathrm{T}$ generates a straight line with a slope of E_a/R (Fig. 8). The total plot could not be fitted by the Arrhenius equation but two linear sections were obtained in the linearized representation. The values of the

constants were strongly dependent on the temperature range, with much higher adsorption affinity observed at the lower range of temperature (for Zn(II), 0.9929>0.7896; for Pb(II), 0.9692>0.6154). Although not ideal, the model could be treated in two steps to define the limit of E_a, which may echoing the research of adsorption mechanisms (intraparticle diffusion and surface diffusion). The adsorption activation energy of Zn(II) was range from 11.71 kJ $mol^{-1}$to 46.37 kJ mol^{-1}.The adsorption activation energy of Pb(II) was range from 0.26 kJ mol^{-1} to 17.67 kJ mol^{-1}.

3.5 Adsorption mechanisms

To optimize adsorption systems, a detailed understanding of the adsorption mechanism help obtain information regarding trace and structural change. To simplify the process, we assumed that adsorption has nothing to do with the overall rate. The overall rate will be controlled by the rate-limiting step, which may be either surface diffusion, intraparticle diffusion or both. No matter how complicated, surface diffusion will be one of the processes. The Weber–Morris intraparticle diffusion model is the most popular technique for identifying whether intraparticle diffusion is the rate-limiting step [65-67].

Plots of q_t versus $t^{0.5}$ are shown in Fig. 9 at 288K, 293K, 298K, 303K and 313K. Each plot has been separated into three linear sections over the entire adsorption process according to the value of x axis (the first segment (0-2), the second segment (2-6), the third segment (6-12)), suggesting three corresponding phases (surface or film diffusion, intraparticle or pore diffusion, final equilibrium). Reports indicate that intraparticle diffusion is the only rate-limiting step when the plot passes through the origin [63]. In this case, the plot did not pass through the origin' therefore, intraparticle diffusion is not the sole rate-limiting step [16]. The scope of the second segment represented the rate of intraparticle diffusion, while the first represented the surface diffusion with a faster rate than the one that followed (Fig. 9a and 9b). The intercept of the second segment is related to the thickness of the boundary layer, and a larger intercept suggests that surface diffusion plays a larger role during the rate-limiting step [28]. Therefore, surface diffusion is involved during adsorption concurrent with intraparticle diffusion and is related to the adsorption rate. For Zn(II), the lower intercept value indicates that surface diffusion became less important when increasing the temperature [64] because the more strenuous molecular thermal motion promoted surface diffusion and the migration of metal ions from the bulk of the solution to the surface of the nZVI-Mont [28]. However, this change shifted for Pb(II), may due to a

379 combination of rapidness and randomness that caused opposing effects of molecular thermal
380 motion.

381 ### 3.6 Thermodynamic studies

382 Accurate thermodynamic parameters might affect the utility of the measured data and help reveal
383 the causes of the adsorption phenomena. Moreover, these parameters can provide useful
384 information to predict laboratory findings at a broad range of temperatures. The adsorption
385 capacity of nZVI-Mont and the decrease in rate observed when increasing the temperature
386 indicated that the adsorption of Zn(II) and Pb(II) on nZVI-Mont was exothermic (Fig. 3); the
387 attractive forces between nZVI-Mont and ions decrease when the temperature increases. Similar
388 results have been noted by earlier studies for different adsorbent [68, 69]. It may be explained as
389 below: When nZVI-Mont was introduced to solution containing Zn(II) or Pb(II), ions can be
390 immobilized probably depending upon the increasing of pH [70] . Zn(II) and Pb(II) may also be
391 removed by precipitation [70], and the increasing of molecular thermal motion, leads to more
392 $Zn(OH)_2$ and $Pb(OH)_2$ on the oxidized nZVI surface as the passivation layer which may be a
393 possible reason why the adsorption of Zn(II) and Pb(II) on nZVI-Mont decrease with the increase
394 in temperature.
395 K_o was estimated from a plot of $\ln(C_s/C_e)$ versus C_s (Fig. 10a, 11a) when C_s approaches zero
396 [36, 50]. The Gibbs free energy (ΔG^o) and the enthalpy of adsorption (ΔH^o) were calculated using
397 K_o. The entropy of adsorption (ΔS^o) was obtained from the slope and intercept of $\ln K_0$ versus
398 $1/T$ (Fig. 10b and 11b). The relevant thermodynamic parameters are displayed in a specific order
399 (Tab. 3). K_o decreased when increasing the temperature, indicating that the adsorption was
400 exothermic. The adsorption of Zn(II) and Pb(II) on nZVI-Mont was spontaneous based on the
401 negative ΔG^o values. The spontaneity decreased when the temperature increased. The data
402 suggest that the adsorption on nZVI-Mont was easier for Zn(II) than Pb(II) under same conditions,
403 as shown by the lower ΔG^o values (Tab. 3). The standard enthalpy change (ΔH^o) for Zn(II) and
404 Pb(II) adsorption were -124.51 and -87.98 kJ mol^{-1}, respectively; the negative values proved that
405 the processes were exothermic. The negative standard entropy change (ΔS^o) for the adsorption of
406 Zn(II) and Pb(II) was -0.34 J mol^{-1} K^{-1} and -0.23 J mol^{-1} K^{-1} respectively. In addition, the
407 randomness of the system decreased during adsorption, as indicated by the negative ΔS^o value
408 [71, 72].

3.7 Discussion of the adsorption mechanism

Zero-valent iron nanoparticles often display a core–shell structure: the core is zero-valent iron, and the shell is composed of iron oxide [56]. Nanoscale iron has higher standard reduction potentials than iron, which might reduce ions by forming an electron source. However, the shell could capture adsorbate ions through surface complexation with the hydroxyl groups formed at the interface [30]. Based on the structural model, the electronic subscription ability of nZVI and the contribution of the surface FeOOH groups in aqueous media can affect the reactivity of the particles [73]. The standard electrode potential (SEP) of Zn(II) (=–0.7618 V, 298 K) is much smaller than that of Fe(II) (=–0.447 V, 298 K); therefore, Zn^0 formation through a redox reaction is highly unlikely. The standard electrode potential (SEP) of Pb(II) (=–0.1263 V, 298 K) [74] is much more positive than that of Fe(II) (=–0.4402 V, 298 K) [30]; therefore, a redox reaction that forms Pb^0 is actually feasible. Recently, the adsorption mechanisms for various metal ions on nZVI-Mont or nZVI were studied [75, 76]. According to these studies, ions with SEP smaller than that of Fe(II), such as Zn(II) and Cd(II), did not exhibit changes in their valence state when fixed on a nZVI surface [56]. Consequently, the mechanism for the adsorption of Zn(II) on nZVI-Mont is very different from that for Pb(II). During Zn(II) adsorption, the groups in the nZVI shell (e.g., Fe_3O_4, Fe_2O_3, FeOOH) or montmorillonite might fix the ions through Van der Waals forces, magnetic interactions forces, and/or surface complexation. Pb(II) in solution can be reduced to Pb^0 on the nZVI-Mont surface through an electrochemical process [77, 78]. The mechanism for Pb(II) removal using nZVI-Mont, is similar to that of nZVI supported by kaolin. Pb(II) ions are absorbed on the surface of nZVI-Mont because the montmorillonite and iron oxides shell can absorb Pb(II), which can be converted to Pb^0 through the reduction of Fe^0 [79]:

$$Fe^0 + 2H_2O + 1/2O_2 \longrightarrow Fe^{2+} + 4OH^- \text{ (in basic solution)} \quad (17)$$

$$Fe^0 + 2H_2O \longrightarrow Fe^{2+} + H_2 + 2OH^- \text{ (in acid solution)} \quad (18)$$

$$Pb^{2+} + \text{Montmorillonite} \longrightarrow Pb^{2+} - \text{Mont (adsorption)} \quad (19)$$

$$Pb^{2+} + Fe_xO_yH_z \longrightarrow Pb^{2+} - Fe_xO_yH_z \text{ (adsorption)} \quad (20)$$

$$Pb^{2+} - \text{Mont (or } Pb^{2+} - Fe_xO_yH_z) + 2e \longrightarrow Pb^0 - \text{Mont (or } Pb^0 - Fe_xO_yH_z) \quad (21)$$

4. Conclusions

Montmorillonite-supported zero-valent iron nanoparticles are an effective adsorbent for heavy metal ions in contaminated water. The adsorption of aqueous Zn(II) and Pb(II) by nZVI-Mont was

investigated on a lab scale. In this work, positive results were obtained as follows.

(i) The adsorption of Zn(II) and Pb(II) on nZVI-Mont was exothermic. When increasing the temperature, the adsorption capacity of Zn(II) and Pb(II) was smaller, and the adsorption rate decreased. The equilibrium time for Zn(II) adsorption was approximately 40 min, which was much shorter than that for Pb(II).

(ii) A pseudo-second-order kinetic model fits the adsorption process for Zn (II) and Pb (II) on nZVI-Mont better than the pseudo-first-order kinetics model. These species were adsorbed onto the surface through a chemical interaction. The rate-limiting step involved surface adsorption and intraparticle diffusion.

(iii) The adsorption of Zn(II) on nZVI-Mont was simultaneously physical and chemical, fitting the Freundlich, Temkin and the D–R isotherm models. The Langmuir isotherm model cannot describe this process. However, the adsorption of Pb(II) on nZVI-Mont primarily involves chemisorption, fitting the Freundlich isotherm model; the other three model cannot describe it appropriately.

(iv) The activation energies of the Zn(II) adsorption onto nZVI-Mont was range from 11.71 kJ mol^{-1} to 46.37 kJ mol^{-1} and the activation energies of the Pb(II) adsorption onto nZVI-Mont was range from 0.26 kJ mol^{-1} to 17.67 kJ mol^{-1}, which may correspond with two adsorption mechanisms (intraparticle diffusion and surface diffusion).

(v) The negative values for the Gibbs free energy (ΔG^o) and enthalpy of adsorption (ΔH^o) that the adsorption process was spontaneous and exothermic. The adsorption of Zn(II) on nZVI-Mont was easier than that of Pb(II) under the same conditions. The negative standard entropy change (ΔS^o) indicated that nZVI-Mont had a better affinity for Pb(II) than Zn(II).

(vi) The adsorption mechanism for Zn(II) is significantly different from that for Pb(II). The montmorillonite or groups in the shell of nZVI may fix the Zn(II) ion to the surface of nZVI-Mont. The Pb(II) irons will be converted to Pb^0 through the reduction of Fe^0 or absorbed on the surface of nZVI-Mont because montmorillonite and iron oxides shell can absorb Pb(II).

Compared with previous works, we emphasized the way and the mechanism of Zn(II) and Pb(II) adsorption based on the data of kinetics and isotherm and discussed the thermodynamic characteristics. The optimizing of preparation conditions for nZVI-Mont is needed to be focused on in future, as well as a pilot-scale study.

Acknowledgments

This work was financially supported by the Program for National Key Technology Research and Development Program, Ministry of Science and Technology, China (Grant no. 2010BAC10B02) and the Key Program for Science and Technology Development of Anhui Province (No. 12010402111). We thank the editors and reviewers for their help polishing the paper and in-depth discussions.

References

[1] S. Tunali, A. Cabuk and T. Akar, *Chemical Engineering Journal*, 2006, **115**, 203-211.

[2] P. Kikot, M. Viera, C. Mignone and E. Donati, *Hydrometallurgy*, 2010, **104**, 494-500.

[3] X.L. Pan, J.L. Wang and D.Y. Zhang, *Process Biochemistry*, 2005, **40**, 2799-2803.

[4] V. Murphy, H. Hughes and P. McLoughlin, *Water Research*, 2007, **41**, 731-740.

[5] W.B. Achiba, N. Gabteni, A. Lakhdar, G.D. Laing, M. Verloo, N. Jedidi and T. Gallali, *Agriculture Ecosystems Environment*, 2009, **130**, 156-163.

[6]G. Zengin, *Environmental Earth Sciences*, 2013, **70**, 3031-3041.

[7] M. Trgo, J. Perić and N.V. Medvidović, *Journal of Environment Management*, 2006, **79** 298-304.

[8] D. Ozdes, C. Duran and H.B. Senturk, *Journal of Environment Management*, 2011, **92**, 3082-3090.

[9] Jerome O. Nriagu, *Zinc in the Environment*, Part I. Ecological Cycling, John Wiley and Sons, 1980.

[10] B.E. Clayton, *British medical bulletin*, 1975, **31**, 236-240.

[11] H. Mielke, *American scientist*, 1999, **87**, 62-73.

[12] USEPA, Priority pollutants, *code of federal regulations*, Title 40: protection of environment, chap I, Appendix A to 40 CFR Part 423, Environmental Protection Agency, 2005.

[13] R.P. Schwarzenbach, T. Egli, T.B. Hofstetter, U. Von Gunten and B. Wehrli, *Annual Review of Environment and Resources*, 2010, **35**, 109-136.

[14] M. Revathi, M. Saravanan, A.B. Chiya and M. Velan, *Clean Soil Air Water*, 2012, **40**, 66-79.

[15] S. Ahmady-Asbchin and N. Jafari, *Water Science & Technolog* , 2013, **68**, 1384-1390.

[16] T.K. Sen and D. Gomez, *Desalination*, 2011, **267**, 286-294.

[17] S. Saraswat and J.P.N. Rai, *International Journal of Mineral Processing*, 2010, **94,** 203-206.

[18] K. Aftab, K. Akhtar, A. Jabbar, I. H. Bukhari and R. Noreen, *Water Research*, 2013, **47**,

4238-4246.

[19] L. Giraldo, A. Erto and J.C. Moreno-Pirajan, *Adsorption-Journal of The International Adsorption Society*, 2013, **19**, 465-474.

[20] M. Lee, I.S. Paik, I. Kim, H. Kang and S. Lee, *Journal of Hazardous Materials*, 2007, **144**, 208-214.

[21] S. Kolemen, N.B. Acarali, N. Tugrul, E.M. Derun and S. Piskin, *Water Air and Soil Pollution*, 2013, **224**, 1367.

[22] S.A. Kim, S. Kamala-Kannan, K. Lee, Y. Park, P.J. Shea, W. Leed, H. Kim and B. Oh, *Chemical Engineering Journal*, 2013, **217**, 54-60.

[23] A. Erto, L. Giraldo, A. Lancia and J.C. Moreno-Pirajan, *Water Air and Soil Pollution*, 2013, **224**, 1531-1538.

[24] H. Zhu, Y. Jia, X. Wu and H. Wang, *Journal of Hazardous Materials*, 2009, **172**, 1591-1596.

[25] K. Gupta, K. Biswas and U.C. Ghosh, *Industrial & Engineering Chemistry Research*, 2008, **47**, 9903-9912.

[26] J. Wei, X. Xu, Y. Liu and D. Wang, *Water Research*, 2006, **40**, 348-354.

[27] X.Q. Li and W.X. Zhang, *Journal of Chemical Physics C*, 2007, **111**, 6939-6946.

[28] H.K. Boparai, M. Joseph and D.M. O'Carroll, *Journal of Hazardous Materials*, 2011, **186**, 458-465.

[29] Q.Y. Liu, Y.L. Bei and F. Zhou, *Central European Journal of Chemistry*, 2009, **7**, 79-82.

[30] C. Üzüm, T. Shahwan, A.E. Erŏglu, K.R. Hallam, T.B. Scott and I. Lieberwirth, *Applied Clay Science*, 2009, **43**, 172-181.

[31] X. Zhang, S. Lin, X.Q. Lu and Z.L. Chen, *Chemical Engineering Journal*, 2010, **163**, 243-248.

[32] D. Wen, Y.S. Ho and X. Tang, *Journal of Hazardous Materials*, 2006, **133**, 252-256.

[33] Y.S. Ho, *Scientometrics*, 2004, **59**, 171-177.

[34] S. Azizian, *Journal of Colloid and Interface Science*, 2004, **276**, 47-52.

[35] S. Lagergren, *Handlingar*, 1898, **24**, 1.

[36] R. Calvet, *Environmental Health Perspectives*, 1989, **83**, 145-177.

[37] D. R. Cox, *Applied statistics*, 1972, **20**, 113-120.

[38] I. Langmuir, *Journal of the American Chemical Society*, 1918, **40**, 1361-1403.

529 [39] C.H. Yang, *Journal of Colloid and Interface Science*, 1998, **208**, 379–387.

530 [40] H. Freundlich, *J. Phys. Chem.*, 1906, **57**, 1100-1107.

531 [41] M.J. Temkin and V. Pyzhev, *Acta Physiochim Chemistry*, 1940, **12**, 217-222.

532 [42] N.D. Hutson and R.T. Yang, *Adsorption*, 1997, **3**, 189-195.

533 [43] M.M. Dubinin and L.V. Radushkevich, *Phys. Chem. Sect.*, 1947, **55**, 327-329.

534 [44] S. Arrhenius, *Z. Phys. Chem.*, 1889, **4**, 226-248.

535 [45] P. Chingombe, B. Saha and R.J. Wakeman, *Journal of Colloid and Interface Science*, 2006,

536 **302**, 408–416.

537 [46] M.M.A. EI-Latif, A.M. Ibrahim and M.F. EI-Kady, *Journal of American Science*, 2010, **6**,

538 267–283.

539 [47] W. J. Jr. Weber and J. C. Morris, *J. Sanit. Eng. Div. Am. Soc. Civ. Engrs.*, 1963, **89**, 31- 59.

540 [48] J.W. Gibbs, Thermodynamics, Dover Publications, 1961.

541 [49] L.G. Hepler, *Journal of the American Chemical Society*, 1963, **85**, 3089-3092.

542 [50] J.W. Biggar and M.W. Cheung, *Soil Science Society of America Journal*, 1973, **37**, 863–868.

543 [51] Z.H. Ai, Z.T. Gao, L.Z. Zhang, W.W. He and J.J. Yin, *Environmental Science & Technology*,

544 2013, **47**, 5344-5352.

545 [52] S.Z. Li, P.X. Wu, H.L. Li, N.W. Zhu, P. Li, J.H. Wu, X.D. Wang and Z. Dang, *Applied Clay*

546 *Science*, 2010, **50**, 330-336.

547 [53] Q. Wang, S. Snyder, J. Kim and H. Choi, *Environ. Sci. Technol.*, 2009, **43**, 8871-8876.

548 [54] Z.X. Chen, T. Wang, X.Y. Jin, Z.L. Chen, M. Megharaj and R. Naidu, *Journal of Colloid and*

549 *Interface Science*, 2013, **398**, 59-66.

550 [55] L.N. Shi, Y.M. Lin, X. Zhang and Z.L. Chen, Synthesis, *Chemical Engineering Journal*, 2011,

551 **171**, 612-617.

552 [56] O. Çelebi, C. Uzum, T. Shahwan and H.N. Erten, *Journal of Hazardous Materials*, 2007, **148**,

553 761-767.

554 [57] Q. Wang, S. Snyder, J. Kim and H. Choi, *Environmental Science & Technology*, 2009, **43**,

555 8871-8876.

556 [58] S.T. Chang and H.T. Chang, *Polym. Degrad. Stab.*, 2001, **71**, 261-266.

557 [59] J.Q. Jiang, C. Cooper and S. Ouki, *Chemosphere*, 2002, **47**, 711-716.

558 [60] M.R. Taha, K. Ahmad, A.A. Aziz and Z. Chik, Geoenvironmental aspects of tropical residual

559 soils, in: B.B.K. Huat, G.S. Sew, F.H. Ali (Eds.), Tropical Residual Soils Engineering, A.A.
560 Balkema Publishers, London, UK, 2009, 377-403.
561 [61] K. Biswas, S.K. Saha and U.C. Ghosh, *Industrial & Engineering Chemistry Research*, 2007,
562 **46**, 5346-5356.
563 [62] A. Kaya and A.H. Ören, *Journal of Hazardous Materials B*, 2005, **125**, 183-189.
564 [63] A. Ozcan, A.S. Ozcan and O. Gok, Adsorption kinetics and isotherms of anionic dye of
565 reactive blue 19 from aqueous solutions onto DTMA-sepiolite, in: A.A. Lewinsky (Ed.),
566 Hazardous Materials and Wastewater—Treatment, Removal and Analysis, Nova Science
567 Publishers, New York, 2007.
568 [64] E.I. Unuabonah, K.O. Adebowale and B.I. Olu-Owolabi, *Journal of Hazardous Materials*,
569 2007, **144**, 386-395.
570 [65] S.I.H. Taqvi, S.M. Hasany and M.Q. Bhanger, *Journal of Hazardous Materials*, 2007, **141**,
571 37-44.
572 [66] D. Kavitha and C. Namasivayam, *Bioresource Technology*, 2007, **98**, 14-21.
573 [67] F.C. Wu, R.L. Tseng and R.S. Juang, *Chemical Engineering Journal*, 2009, **153**, 1-8.
574 [68] S.S. Gupta and K.G. Bhattacharyya, *Journal of Colloid and Interface Science*, 2006, **295**,
575 21-32.
576 [69] T.K. Sen and M.V. Sarzali, *Chemical Engineering Journal*, 2008, **142**, 256-262.
577 [70] D. O'Carroll, B. Sleep, M. Krol, H. Boparai, Christopher Kocur, *Advances in Water*
578 *Resources*, 2013, **51**, 104-122.
579 [71] M.K. Purkait, A. Maiti, S. DasGupta and S. De, *Journal of Hazardous Materials*, 2007, **145**,
580 287-295.
581 [72] B.K. Nandi, A. Goswami and M.K. Purkait, *Journal of Hazardous Materials*, 2009, **161**,
582 387-395.
583 [73] Y. Sun, X. Li, J. Cao, W. Zhang and H.P. Wang, *Advances in Colloid and Interface Science*,
584 2006, **120**, 47-56.
585 [74] M. Ladd, Introduction to Physical Chemistry, third, Cambridge University Press, Cambridge,
586 2004.
587 [75] D.L. Huber, *Small*, 2005, **1**, 482-501.
588 [76] X.Q. Li and W.X. Zhang, *Journal of Chemical Physics C*, 2007, **111**, 6939-6946.

589 [77] S.M. Ponder, J.G. Darab and T.E. Mallouk, *Environmental Science & Technology*, 2000, **34**,
590 2564-2569.
591 [78] S.A. Kim, S. Kamala-Kannan, K. Lee, Y. Park, P.J. Shea, W. Leed,, H. Kim and B. Oh,
592 *Chemical Engineering Journal*, 2013, **217**, 54-60.
593 [79] X. Zhang, S. Lin, Z.L. Chen, M. Megharaj and R. Naidu, *Water Research*, 2011, **45**,
594 3481-3488.

Figure Captions:

Fig. 1, TEM images of montmorillonite and nZVI synthesized on montmorillonite.

Fig. 2, XRD pattern of nZVI-Mont.

Fig. 3, The effect of temperature on the adsorption kinetics of Zn(II) (a) and Pb(II) (b) ions on nZVI-Mont.

Fig. 4, Pseudo first-order kinetic model fit for Zn(II) and Pb(II) adsorption onto nZVI-Mont particles at various temperatures.

Fig. 5, Pseudo second-order kinetics of Zn(II) and Pb(II) adsorption onto nZVI-Mont particles at various temperatures.

Fig. 6, Linearized Freundlich (a), Langmuir (b), Temkin (c), and D-R isotherms (d) for Zn(II) adsorption on nZVI-Mont particles at 298K.

Fig. 7, Linearized Freundlich (a), Langmuir (b), Temkin (c), and D-R isotherms (d) for Pb(II) adsorption on nZVI-Mont particles at 298K.

Fig. 8, Determination of the activation energy for Zn(II) and Pb(II) adsorption on nZVI-Mont particles.

Fig. 9, Intraparticle diffusion plots for Zn(II) and Pb(II) adsorption on nZVI-Mont at different temperatures.

Fig. 10, Plots of ln(Cs/Ce) versus Cs at various temperatures (a) and plot of K_0 versus 1/T for Zn(II) (b).

Fig. 11, Plots of ln(Cs/Ce) versus Cs at various temperatures (a) and plot of K_0 versus 1/T for Pb(II) (b).

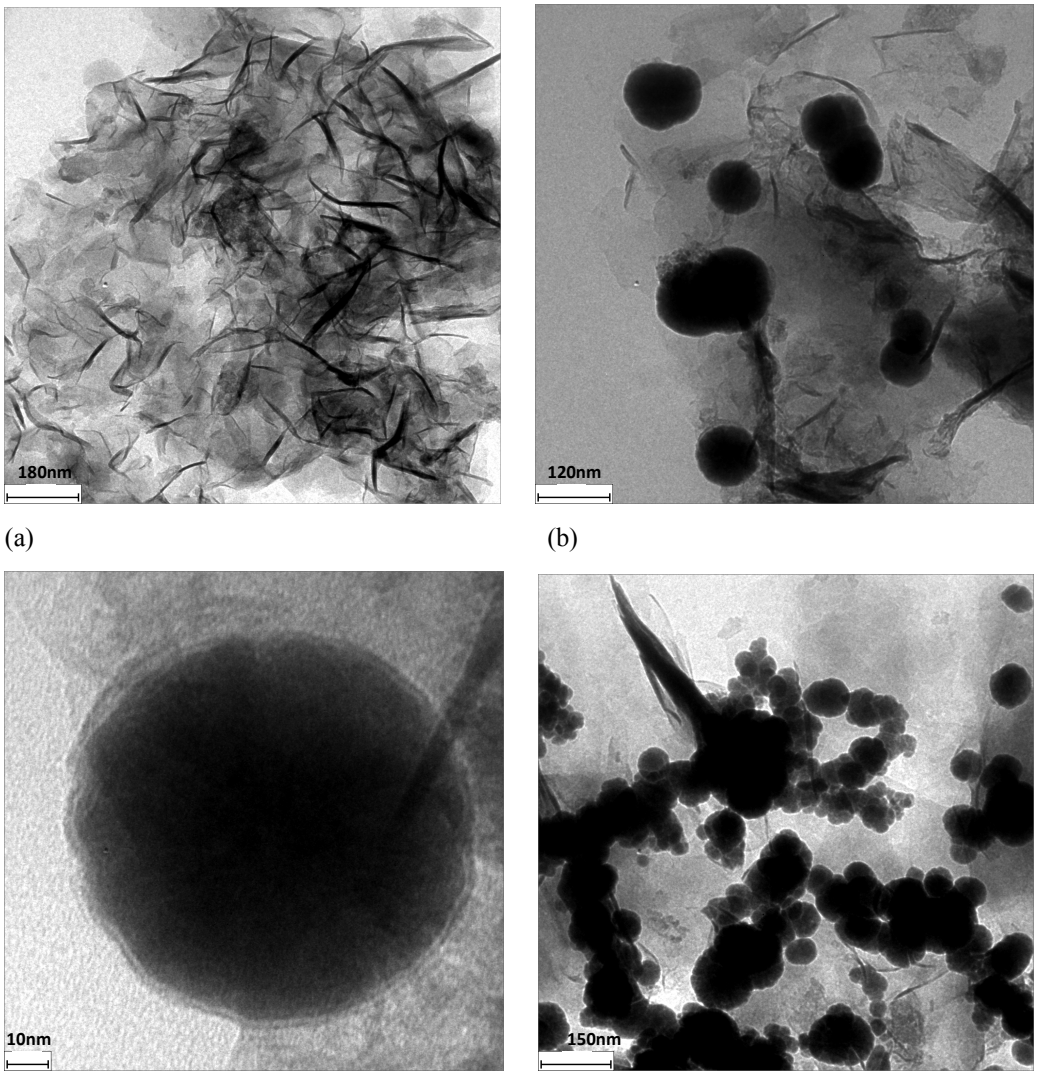

(a) (b)

(c) (d)

Fig. 1 TEM images of montmorillonite and nZVI synthesized on montmorillonite.

(a) montmorillonite; (b) nZVI; (c) The core-shell structure of nZVI; (d) nZVI particles in a chain-like form.

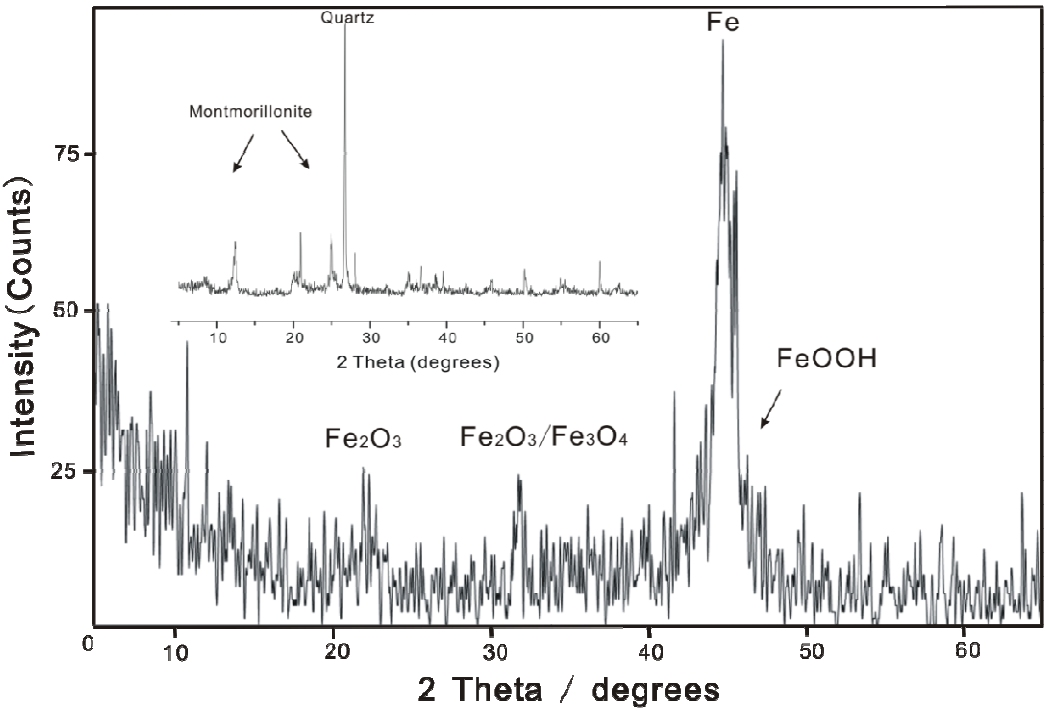

Fig. 2 XRD pattern of nZVI-Mont. The inset shows the pattern of montmorillonite.

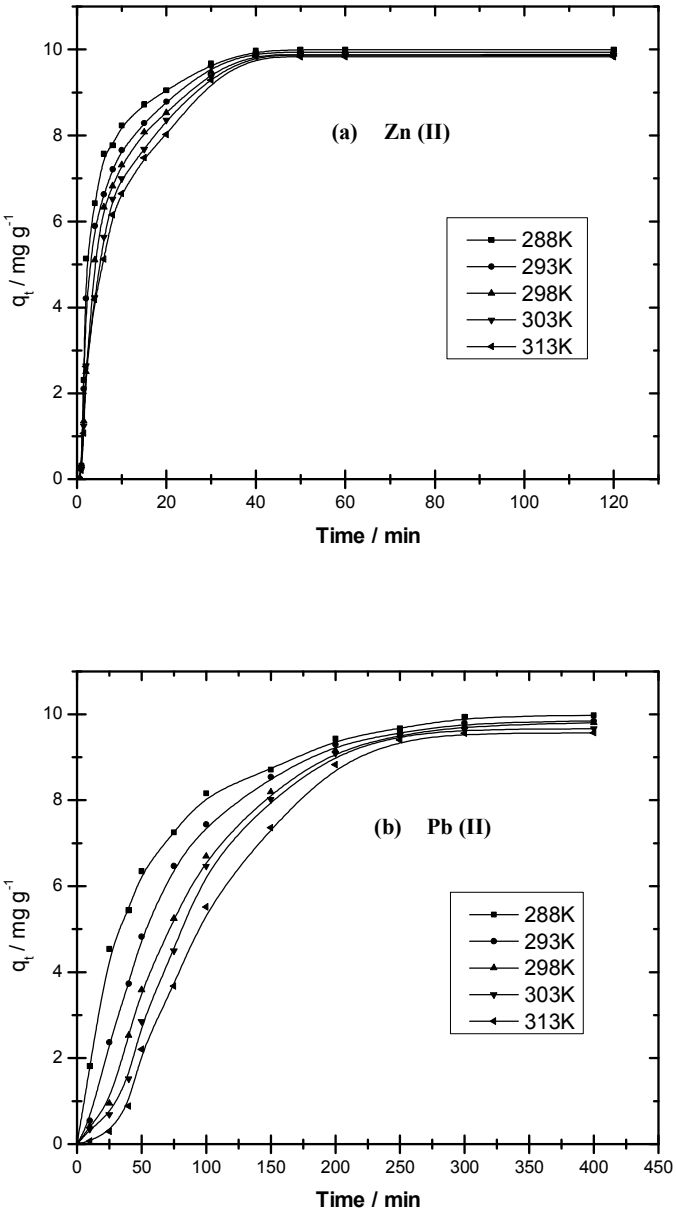

Fig. 3 The effect of temperature on the adsorption kinetics of Zn(II) (a) and Pb(II) (b) ions on nZVI-Mont; pH=5.0, adsorbent dosage=5 g L^{-1}, Initial metal ions concentration=50 mg L^{-1}.

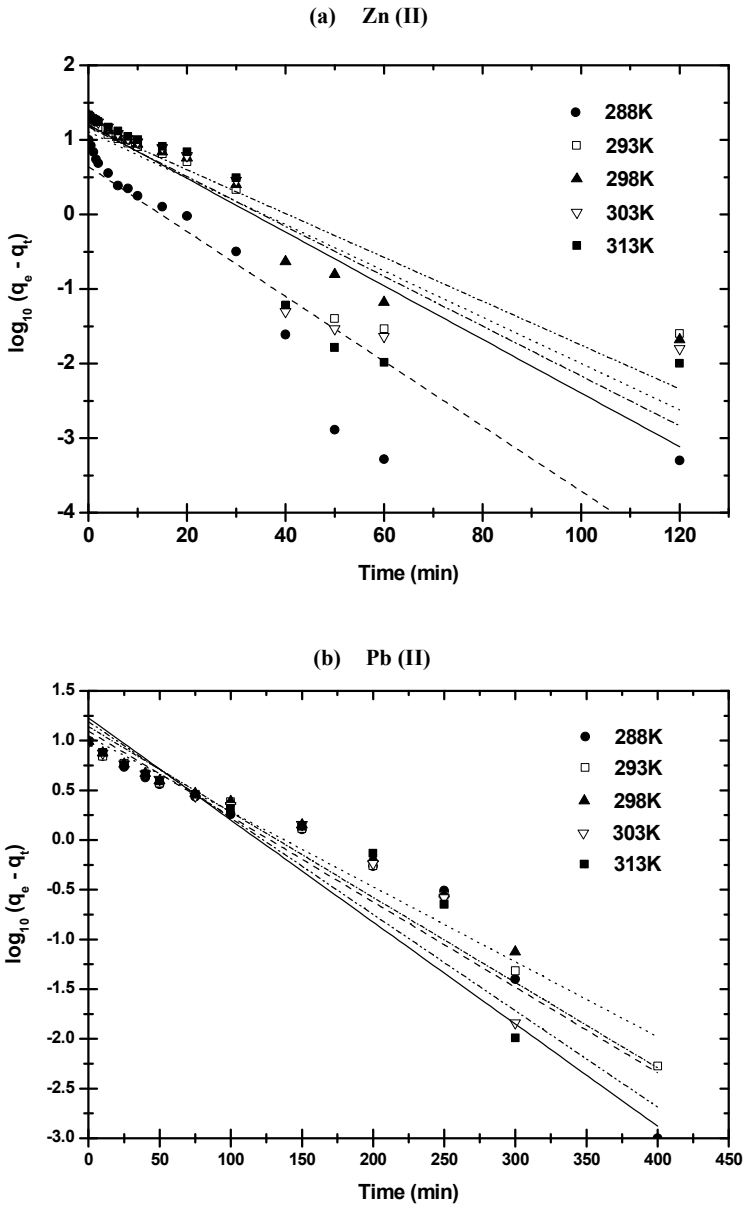

Fig. 4 Pseudo first-order kinetic model fit for Zn(II) and Pb(II) adsorption onto nZVI-Mont particles at various temperatures.

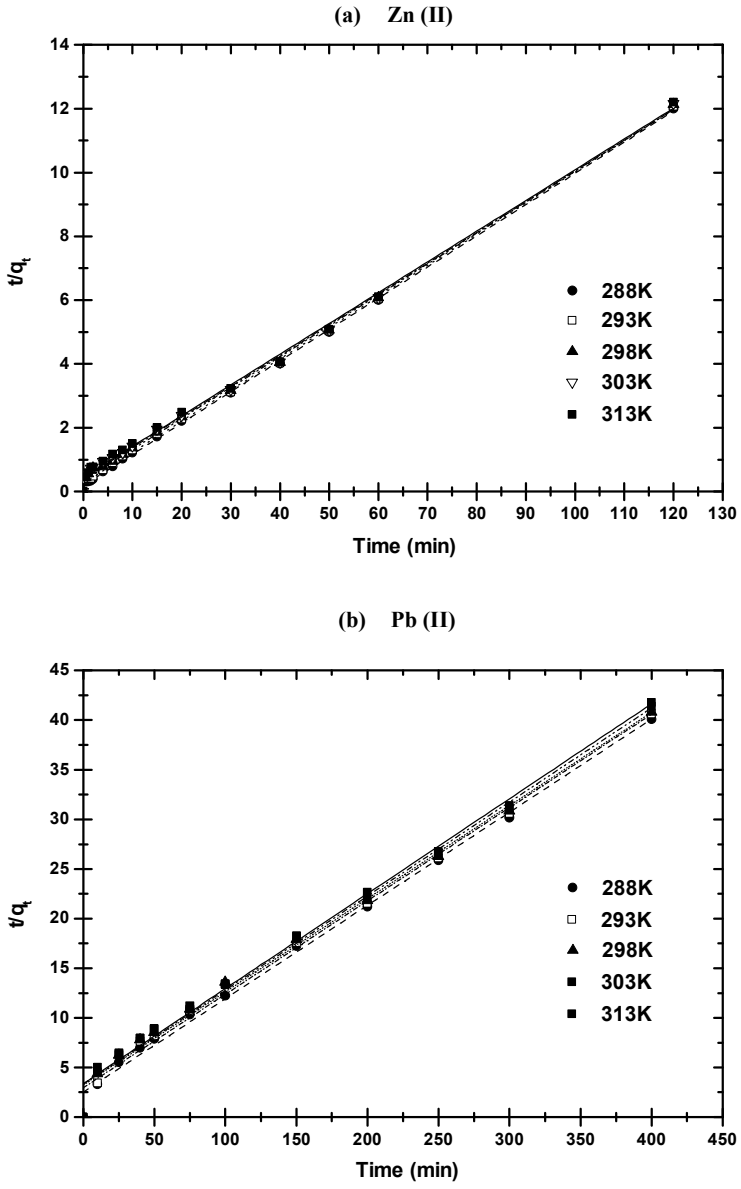

Fig. 5 Pseudo second-order kinetics of Zn(II) and Pb(II) adsorption onto nZVI-Mont particles at various temperatures.

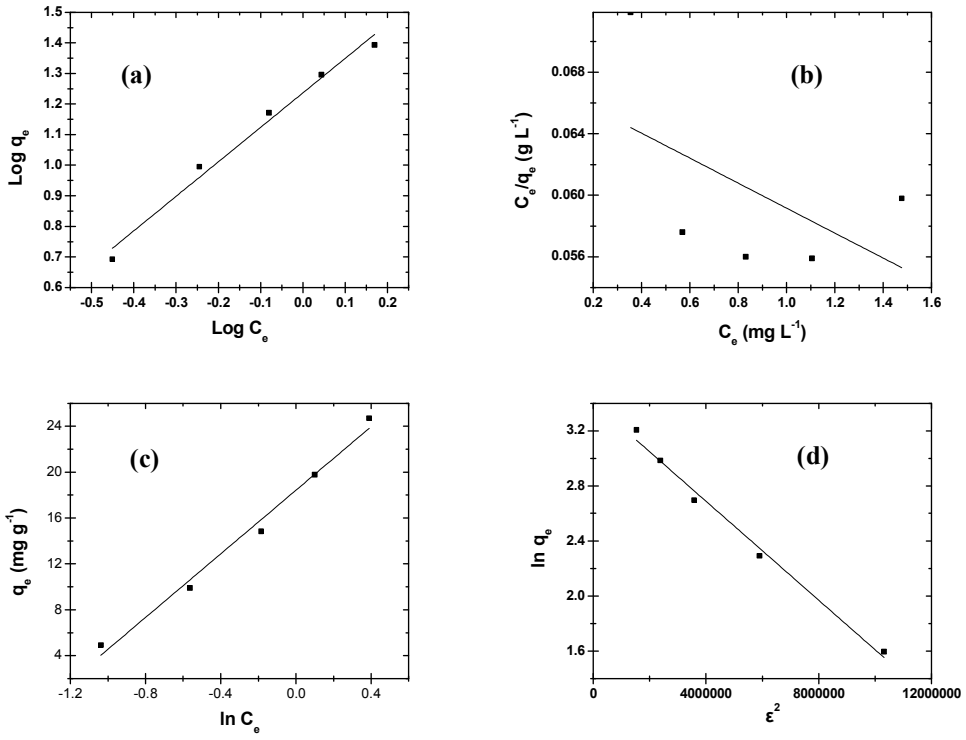

Fig. 6 Linearized Freundlich (a), Langmuir (b), Temkin (c), and D-R isotherms (d) for Zn(II) adsorption on nZVI-Mont particles at 298K.

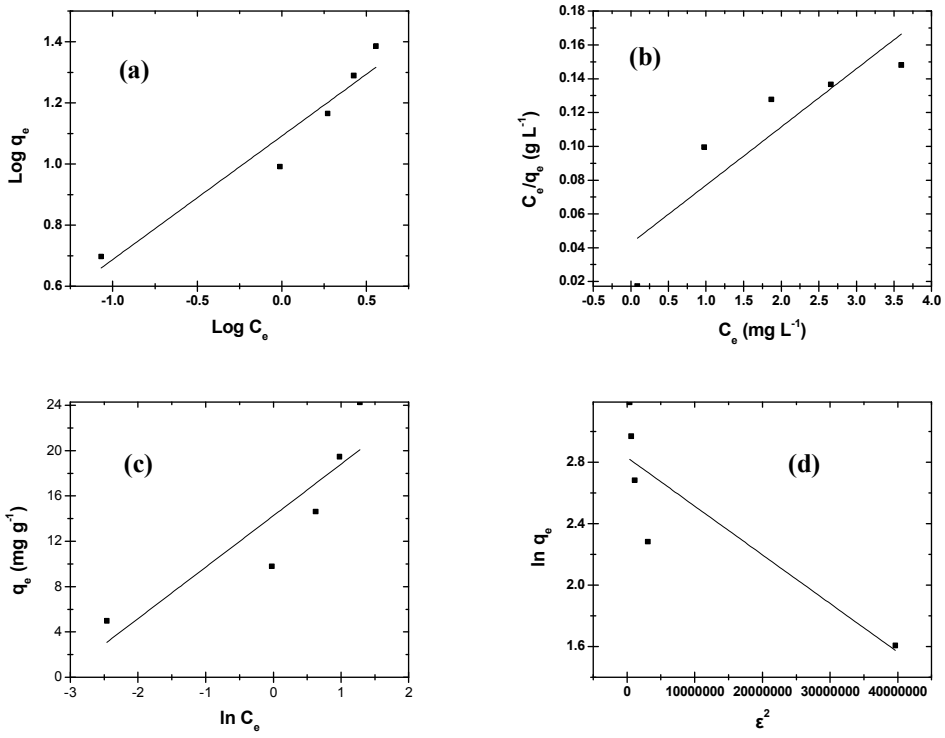

Fig. 7 Linearized Freundlich (a), Langmuir (b), Temkin (c), and D-R isotherms (d) for Pb(II) adsorption on nZVI-Mont particles at 298K.

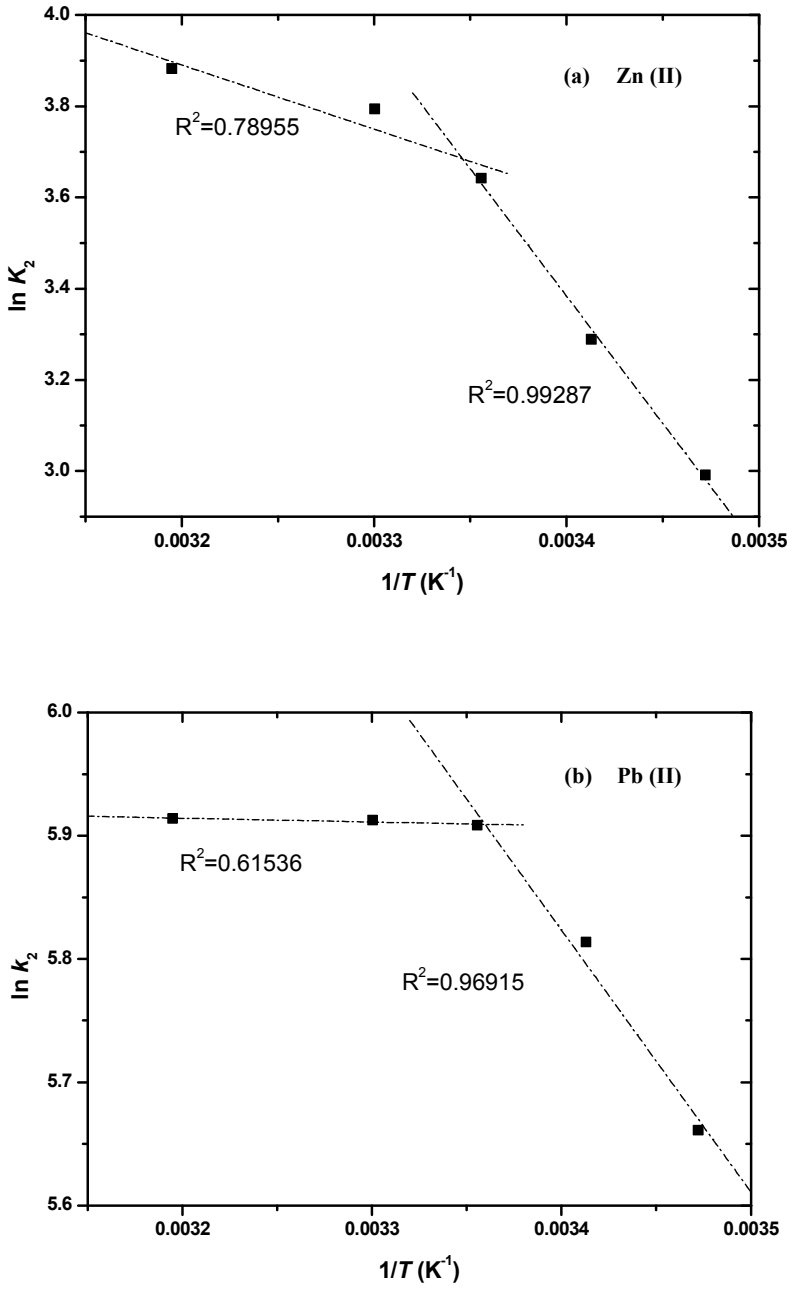

Fig. 8 Determination of the activation energy for Zn(II) and Pb(II) adsorption on nZVI-Mont particles.

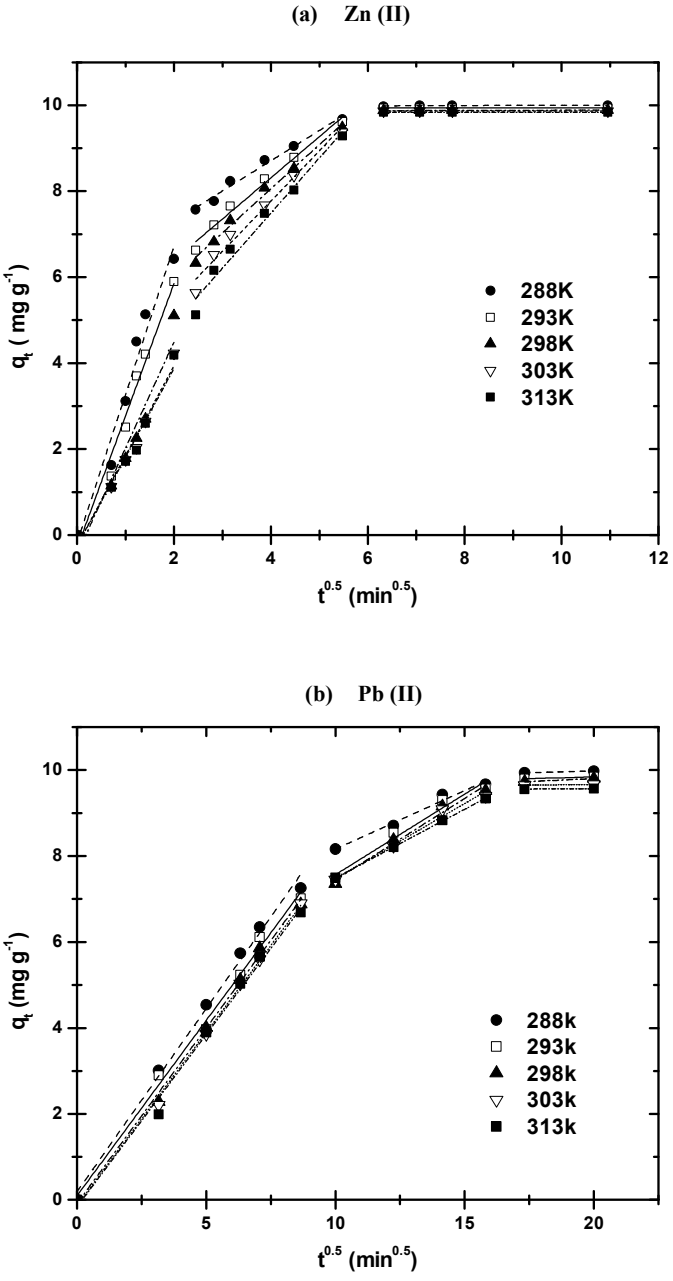

Fig. 9 Intraparticle diffusion plots for Zn(II) and Pb(II) adsorption on nZVI-Mont at different temperatures.

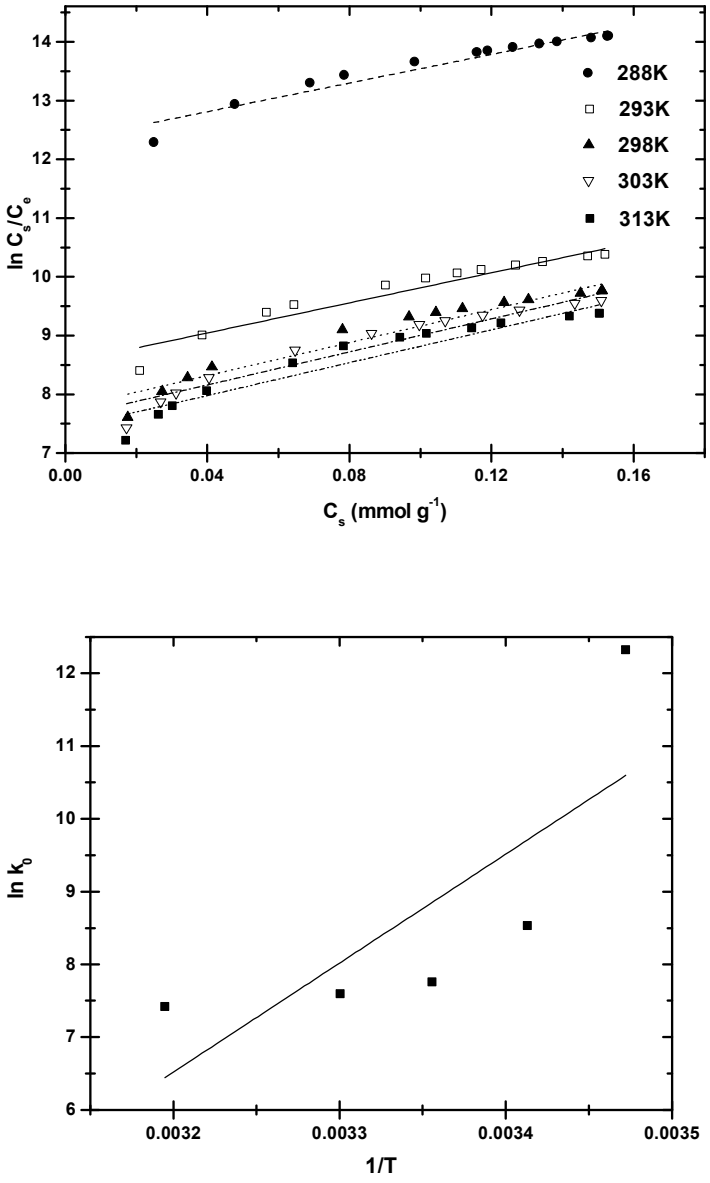

Fig. 10 Plots of ln(Cs/Ce) versus Cs at various temperatures (a) and plot of K_0 versus 1/T (b) for Zn(II).

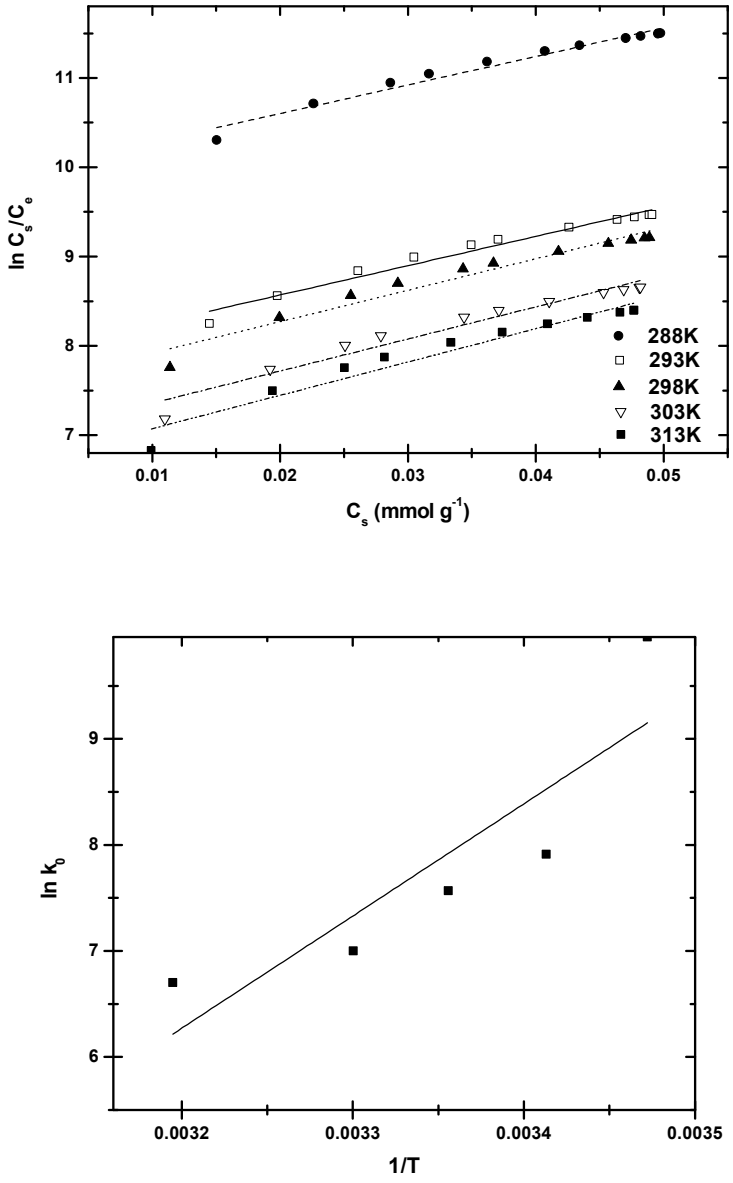

Fig. 11 Plots of ln(Cs/Ce) versus Cs at various temperatures (a) and plot of K_0 versus 1/T (b) for Pb(II).

Table Captions:

Tab. 1, Adsorption kinetic model rate constants for Zn(II) and Pb(II) adsorption on nZVI-Mont particles at different temperatures.

Tab. 2, Langmuir, Freundlich, Temkin, and D–R isotherm model parameters and correlation coefficients for adsorption of Zn(II) and Pb(II) on nZVI-Mont particles at 298K.

Tab. 3, Thermodynamic parameters for adsorption of Zn(II) and Pb(II) onto nZVI-Mont particles.

Tab. 1

Adsorption kinetic model rate constants for Zn(II) and Pb(II) adsorption on nZVI-Mont particles at different temperatures.

Adsorbate	Temperature (K)	$q_{e,exp}$ (mg g^{-1})	Pseudo first-order			Pseudo second-order			
			k_1 (min^{-1})	$q_{e,cal}$ (mg g^{-1})	r_1^2	k_2 (g mg^{-1} min^{-1})	$q_{e,cal}$ (mg g^{-1})	h (mg g^{-1} min^{-1})	r_2^2
Zn(II)	288K	9.9985	0.1002	4.36	0.8200	0.0502	10.2229	5.2416	0.9994
	293K	9.9384	0.1073	4.57	0.7701	0.0373	10.2428	3.9159	0.9989
	298K	9.8862	0.1015	6.02	0.8843	0.0262	10.3295	2.7920	0.9977
	303K	9.8662	0.1155	5.79	0.7790	0.0225	10.3745	2.4220	0.9970
	313K	9.8338	0.1243	6.34	0.7801	0.0206	10.3788	2.2151	0.9964
Pb(II)	288K	9.9798	0.0198	12.44	0.9210	0.0035	10.6428	287.4945	0.9938
	293K	9.8483	0.0174	10.93	0.9674	0.0030	10.6259	334.8903	0.9909
	298K	9.8048	0.0198	13.79	0.9018	0.0027	10.6553	368.1534	0.9904
	303K	9.6644	0.0223	15.54	0.9089	0.0027	10.5508	369.6347	0.9900
	313K	9.5692	0.0237	16.89	0.8928	0.0027	10.4548	370.1419	0.9901

Tab. 2

Langmuir, Freundlich, Temkin, and D–R isotherm model parameters and correlation coefficients for adsorption of Zn(II) and Pb(II) on nZVI-Mont particles at 298K.

Adsorbate	Isotherm	Parameters		r^2
Zn(II)	Freundlich	K_F	n	0.981
		17.25	0.89	
	Langmuir	q_m(mg g^{-1})	K_L(L mg^{-1})	0.048
		-123.15	-0.12	
	Temkin	K_T	b	0.983
		3.78	178.66	
	D – R	q_d	β	0.988
		30.20	0.00	
Pb(II)	Freundlich	K_F	n	0.922
		12.35	2.47	
	Langmuir	q_m(mg g^{-1})	K_L(L mg^{-1})	0.746
		29.04	0.51	
	Temkin	K_T	b	0.732
		23.09	545.13	
	D – R	q_d	β	0.677
		16.95	0.00	

Tab. 3

Thermodynamic parameters for adsorption of Zn(II) and Pb(II) onto nZVI-Mont particles.

Adsorbate	Temperature (K)	K_o	ΔG^o (kJ mol^{-1})	ΔH^o (kJ mol^{-1})	ΔS^o (J mol^{-1} K^{-1})
Zn(II)	288K	224329.2236	-29.5015	-124.5136	-0.3442
	293K	5075.6506	-20.7845		
	298K	2337.3194	-19.2179		
	303K	1992.2900	-19.1380		
	313K	1668.9667	-19.3088		
Pb(II)	288K	21208.7688	-23.8537	-87.9766	-0.2294
	293K	2734.3253	-19.2776		
	298K	1934.3565	-18.7491		
	303K	1097.6535	-17.6363		
	313K	813.1617	-17.4377		

Jiao Wang

Born in 1989.06.29, female, at CAS Key Laboratory of Crust-Mantle Materials and the Environments, School of Earth and Space Sciences, University of Science and Technology of China

2008- 2012: Obtain Bachelor of Science Degree from the Inner Mongolia University at Environmental Science.

2012.9- Present Date: Work as the undergraduate PhD in the USTC, Hefei.

The main research area is Mining Waste Comprehensive Utilization Technology, The Harmless Treatment and Depth Using of Mining Solid Waste in Huaibei and Huainan and the rule of gangue leaching filtrate in the transition and transform process in groundwater environmental.